Convective Momentum Transport and its Impact on the Madden-Julian Oscillation in E3SM-MMF

Qiu Yang[1], Walter M. Hannah[2], L. Ruby Leung[1]

[1]Atmospheric Sciences and Global Change Division, Pacific Northwest National Laboratory, Richland, Washington, USA

[2]Lawrence Livermore National Laboratory, Livermore, CA, USA

Key Points:

- CMT affects large-scale circulation and convective organization, and representing CMT reduces model biases in E3SM-MMF simulations.
- ESMT scheme captures the spatial pattern of CMT comparable to 3-D CRMs that explicitly model CMT.
- CMT damps the free tropospheric circulation associated with the MJO, but accelerates its near-surface winds.

Corresponding author: Qiu Yang, qiu.yang@pnnl.gov

Abstract

Convective momentum transport (CMT) is the process of vertical redistribution of horizontal momentum by small-scale turbulent flows from moist convection. Traditional general circulation models (GCMs) and their multiscale modeling framework (MMF) versions poorly represent CMT due to insufficient information of subgrid-scale flows at each GCM grid. Here the explicit scalar momentum transport (ESMT) scheme for representing CMT is implemented in the Energy Exascale Earth System Model-Multiscale Modeling Framework (E3SM-MMF) with embedded 2-D cloud-resolving models (CRMs), and verified against E3SM-MMF simulations with 3-D CRMs and observations. The results show that representing CMT by ESMT helps reduce climatological mean precipitation model bias over the western Pacific and the ITCZ regions, which is attributed to the weakened mean easterlies over the Pacific. Also, CMT from simulations with 2-D and 3-D CRMs impose a similar impact on Kelvin waves by reducing their variability and slowing down their phase speed, but opposite impacts on the MJO variability. The ESMT scheme readily captures the climatological mean spatial patterns of the zonal and meridional components of CMT and their variability across multiple time scales, but shows some differences in estimating its magnitude. CMT mainly affects the Madden-Julian Oscillation (MJO) by decelerating its winds in the free troposphere, but accelerates its near-surface winds. This study serves as a prototype for implementing CMT scheme in the MMF simulations, highlighting its crucial role in reducing model bias in mean state and spatiotemporal variability.

Plain Language Summary

Small-scale turbulent flows from moist convection typically lead to the vertical redistribution of large-scale winds (referred to as CMT). Due to the coarse grids that are too large to resolve small-scale flows, traditional earth system models poorly represent the CMT, and thus rely on parameterizations that empirically describe the magnitude and vertical profiles of the CMT. In contrast, the default E3SM-MMF is an earth system model with a 2-D (one horizontal dimension and one vertical dimension) cloud-resolving model embedded within each coarse grid so as to better resolve small-scale flows, although it still lacks the necessary information to fully calculate CMT due to the lack of the third dimension. Here we implemented the ESMT scheme to represent CMT in the E3SM-MMF associated with 2-D small-scale flows at each coarse grid. The results show that in general CMT helps reduce model biases in predicting time-mean precipitation and winds as well as the spatiotemporal

variability of tropical convection. The ESMT scheme reproduces the spatial patterns of CMT as simulated by the E3SM-MMF model with 3-D small-scale flows. Lastly, we focused on the MJO, the dominant intraseasonal variability in the tropics, as an example to investigate the impact of CMT.

1 Introduction

CMT refers to vertical redistribution of horizontal momentum of environmental flow by convective updrafts and downdrafts. Early observational studies on the effects of CMT date back to 1980s. For example, LeMone (1983) found that the vertical transport of horizontal momentum normal to a line of cumulonimbus observed during GARP Atlantic Tropical Experiment (GATE) was against the vertical momentum gradient, contrary to the predictions of mixing-length theory. Based on an idealized dynamical model and instrumented aircraft data, LeMone and Moncrieff (1994) investigated the effects of quasi-two-dimensional convective bands on environmental flow through the vertical transport of horizontal momentum. Tung and Yanai (2002a) studied the effects of CMT over the western Pacific warm pool during the Tropical Ocean and Global Atmosphere Coupled Ocean-Atmosphere Response Experiment (TOGA COARE) through momentum budget analysis and concluded that the momentum transport generally induces frictional deceleration and downgradient energy transfer, converting kinetic energy from the large-scale motion to convection and turbulence. By focusing on organized tropical convection such as the Madden-Julian oscillation (MJO), tropical waves, squall and nonsquall mesoscale convective systems, and the diurnal cycle, Tung and Yanai (2002b) found countergradient momentum transport and upscale energy transfer associated with squall lines and westerly wind bursts.

Meanwhile, the development of numerical models and computing resources has allowed detailed analysis of the effects of CMT on environmental flows. For example, Oh, Jiang, Waliser, Moncrieff, and Johnson (2015) analyzed the CMT associated with the MJO based on the NOAA Climate Forecast System Reanalysis and confirmed that it tends to damp the MJO circulation in the free troposphere, while enhancing MJO winds near the surface. By examining the data from a global model with a 7km horizontal mesh, Cheedela and Mapes (2019) concluded that CMT on average exerts a damping effect on vertical wind shear over warm tropical oceans, but countergradient effects do occur locally due to organized convection. Woelfle et al. (2018) compared simulations of the superparameterized Community Earth System Model version 1 (CESM1) with/without momentum transport and concluded

that convective momentum fluxes may be an underappreciated mechanism for controlling the strength of the equatorial cold tongue.

Coarse-resolution GCMs cannot explicitly resolve subgrid-scale momentum fluxes and thus rely on parameterizations to incorporate the effects of CMT. In general, CMT is parameterized as an added drag on the mean flow by adding the resulting tendency into the zonal and meridional momentum equations, providing cumulus friction effects in each GCM grid cell containing convection (Richter & Rasch, 2008). The largest uncertainty in such a parameterization lies in estimation of the in-cloud horizontal velocity, which was assumed to depend only on lateral entrainment and detrainment rate in early studies (e.g., Schneider & Lindzen, 1976) and also influenced by in-cloud pressure gradients in later studies (G. J. Zhang & Cho, 1991b, 1991a; Wu & Yanai, 1994; Kershaw & Gregory, 1997; Gregory et al., 1997). Recent studies concluded that GCMs including CMT parameterizations do show some improvements in simulating large-scale circulation and convective organization. For example, Wu et al. (2003) found that a 20-year GCM simulation with the CMT parameterization successfully reproduces the observed seasonal migration of the ITCZ precipitation across the equator, while those without the CMT parameterization typically fail to capture this feature.

Unlike traditional GCMs, the MMF models with embedded CRMs in each GCM grid cell explicitly resolve subgrid-scale flows, providing a more accurate way to estimate CMT. However, the MMF models with 2-D CRMs cannot represent CMT fully due to the lack of the third dimension, while those with 3-D CRMs are computationally too expensive in practice. There exist several attempts in the literature to address the representation of CMT in the MMF models with 2-D CRMs. For example, Cheng and Xu (2014) proposed an explicit representation of CMT by convective cloud systems including MCSs, where the embedded CRM provides CMT in one horizontal direction and that in the other direction is assumed to be proportional to the vertical mass flux in addition to the effects of entrainment and detrainment. The addition of CMT in an MMF was found to significantly improve the spatial distribution, amplitude, and intraseasonal variability of the surface precipitation in the tropics, and the large-scale circulation patterns. Instead of distinguishing the CMT in one horizontal direction from the other, Tulich (2015) developed a general method, ESMT, for the treatment of CMT in the exact same formalism based on the information provided by the 2-D CRM. The results using a new superparameterized Weather Research and Forecasting model (SP-WRF) showed that the net effect of the formulation is to modestly reduce

the overall strength of the large-scale circulation via cumulus friction effect, and improve the depiction of key synoptic modes of tropical wave variability and time-mean climate. In this study, we adopt the method of Tulich (2015) to introduce CMT in the E3SM-MMF with embedded 2-D CRMs.

The damping effects introduced in the above CMT parameterization mimic the down-gradient momentum transport due to unorganized convection. In contrast, organized convection such as mesoscale convective systems (MCSs) can induce counter-gradient momentum transport, further increasing the complexity of formulating a unified CMT parameterization. Moncrieff (1992) established an archetypal dynamical model for understanding the structure and transport properties of organized convection and expediting its parameterization. Moncrieff (2004) provided an analytic representation of the large-scale organization of tropical convection, highlighting the key role of zonal momentum transport in maintaining the large-scale circulation. Recently, Moncrieff et al. (2017) developed the multiscale coherent structure parameterization (MCSP) to introduce physical and dynamical effects of organized convection that are missing from contemporary parameterizations, which improves the MJO and convectively coupled waves as well as the observed large-scale precipitation patterns in the GCM (Moncrieff, 2019). As inspired by the self-similarity of tropical organized convection (Mapes et al., 2006), Majda (2007) derived a set of multiscale asymptotic models and demonstrated theoretically the key role of CMT in inducing multiscale interactions across mesoscale, synoptic and planetary scales. The central role of CMT in interactions across multiple space and time scales was further studied in a simple dynamical model (Majda & Stechmann, 2009) and an idealized multicloud model (Majda & Stechmann, 2008). Recently, Brenowitz et al. (2018); Yang, Majda, and Brenowitz (2019) used a two-dimensional (2-D) global cloud-resolving model (CRM) to simulate multiscale organization of convection and concluded that CMT from MCSs is the dominant kinetic energy source for planetary-scale zonal winds, promoting planetary-scale organization of convection in the tropics. From a theoretical perspective, Yang and Majda (2017) used a multiscale model to study the upscale impact of MCSs on synoptic-scale equatorial waves in 2-D flows, and extended the results for modeling convectively coupled Kelvin waves (Yang & Majda, 2018) and two-day waves (Yang & Majda, 2019).

In general, vertical shear of horizontal winds affects large-scale organization of convection in several ways, such as the vertical shear-cold pool interaction mechanism for the squall line (the RKW theory, Rotunno et al., 1988), the moisture-stratiform instability for

convectively coupled waves (Majda & Shefter, 2001; Kuang, 2008), and the shear-induced eddy modulation effects for the MJO (Tulich & Kiladis, 2021). By inducing the vertical redistribution of horizontal momentum to enhance/reduce the vertical shear, CMT is found to play a crucial role in affecting large-scale organization of convection such as the MJO. For example, Tung and Yanai (2002b) examined the momentum budget by using the TOGA COARE observations and found that CMT is typically upgradient during the initial westerly wind phase of the MJO but becomes downgradient at the later stage. Kim and Zhang (2021) used a simple analytical approach to interpret the MJO as a new mode of variability, which is forced by Rayleigh damping that is possibly from the CMT. Yang, Majda, and Moncrieff (2019) developed a basic parameterization to mimic the CMT induced by the upshear-moving MCSs embedded in the MJO, and concluded that this parameterization improves key features of the MJO analog in the idealized GCM.

The overall goals of this study are to: 1) investigate the impact of CMT on the simulated climatological mean state and spatiotemporal variability of the large-scale circulation and tropical convection in comparison with observations, 2) assess the skill of the ESMT scheme in representing CMT by comparing E3SM-MMF simulations with 2-D and 3-D CRMs, in which CMT is parameterized by ESMT and explicitly simulated, respectively, 3) document the impact of CMT on the simulated MJO's propagation and vertical structure. The results of this study may serve as a prototype for implementing CMT scheme in the MMF simulations. To achieve these goals, we ran four 10-year E3SM-MMF simulations with embedded 2-D/3-D CRMs and with/without momentum feedback. By comparing these four simulations, we identify the effect of CMT that is parameterized by the ESMT scheme in the 2-D CRM case vs. CMT that is explicitly resolved in the 3-D CRM case, and the effect of the third CRM dimension in influencing large-scale circulation and convective organization. We also verify the skill of the ESMT scheme in representing CMT itself by comparing the 2-D case with the 3-D case in the presence of momentum feedback. Lastly, we focus specifically on the simulated MJO's eastward propagation and vertical structure, and highlight the similarity and discrepancies of CMT effects between the 2-D and 3-D cases.

The rest of the paper is organized as follows. Section 2a summarizes the details of the model setup, while Section 2b outlines the observational and reanalysis data used for comparison. Section 3 discusses the impact of CMT on the simulated large-scale circulation and convective organization, including the climatological mean state and spatiotemporal variability of winds and tropical convection. Section 4 investigates the representation of

CMT by the ESMT scheme by comparing directly its magnitude and vertical structure with the simulations with embedded 3-D CRMs. Section 5 further discusses the impact of CMT on characteristic features of MJO eastward propagation and its vertical structures in both 2-D and 3-D cases. The paper concludes with a discussion in Section 6.

2 Methodology

In this section, we first introduce the E3SM-MMF and then summarize all model setup details for the four simulations. We also outline the observational and reanalysis data used for comparison.

2.1 Model descriptions for E3SM-MMF

E3SM is a state-of-the-science Earth system model that aims at investigating energy-relevant science using code optimized for advanced computers (Golaz et al., 2019). In particular, the atmospheric component of the E3SMv1 is based on the spectral-element atmospheric dynamical core (Dennis et al., 2012) with 72 vertical levels, while its ocean and sea ice components are based on the Model for Prediction Across Scales (MPAS; Ringler et al., 2013; Petersen et al., 2019). GCMs like E3SM parameterize CMT by allowing the parameterized convective updrafts and downdrafts redistribute momentum vertically (Richter & Rasch, 2008). The MMF approach replaces traditional cumulus parameterization by embedding a CRM in each GCM grid, typically providing a better way to represent convection and turbulence. Compared with other MMF models, E3SM-MMF is unique due to its ability to utilize hardware acceleration from GPUs, algorithmic CRM mean-state acceleration, and a reduction in the workload of radiative heating calculations (W. M. Hannah et al., 2020), allowing decadal experiments at 100-km GCM resolution.

The embedded CRM in E3SM-MMF is adapted from the System for Atmospheric Modeling (SAM; Khairoutdinov & Randall, 2003) with a single moment scheme for microphysical processes , a diagnostic Smagorinsky-type closure for subgrid-scale turbulent fluxes, and prescribed aerosol concentrations. The embedded CRM uses a 2-km grid spacing and 10-second time step and either a 32×1 2-D domain in a north-south orientation, or a 32×32 3-D domain. The global cubed-sphere GCM grid is set at ne45pg2 (45×45 elements per cube face and 2×2 physics columns per element), which corresponds to an approximate grid spacing of 100 km. After switching to the new finite volume physics grid E3SM-MMF was found to

Table 1. Summary of four E3SM-MMF simulations conducted in this study. Here "CRM domain" describes the computational domain for CRM simulations at each GCM grid cell, and "Momentum feedback" denotes the tendency of horizontal momentum feedback (MF) from CRM to GCM.

#	Simulation	CRM domain	Momentum feedback
1	MMF2D	32×1 2-D north-south orientated domain	No
2	MMF2DMF	32×1 2-D north-south orientated domain	ESMT
3	MMF3D	32×32 3-D domain	No
4	MMF3DMF	32×32 3-D domain	calculated from CRM flows

produce an unphysical checkerboard pattern on multiple time scales (W. M. Hannah et al., 2022). The checkerboard issue has since been ameliorated by a scheme to transport CRM variance on the GCM grid (W. Hannah & Pressel, 2022). The model is forced by prescribed monthly climatological SST that is representative of Year 2010 and temporally interpolated to give a smooth evolution (Taylor et al., 2000).

In this study, we run four 10-year E3SM-MMF simulations with only differences in the CRM dimension (2-D or 3-D) and momentum feedback (with or without), as shown in Table 1. In all cases, the CRM always feels a momentum feedback tendency from the GCM, which keeps the CRM momentum fields consistent with the parent GCM column. It is worth noting that the momentum feedback in MMF2DMF is represented through the ESMT scheme (Tulich, 2015), while that in MMF3DMF is directly calculated by using the resolved flows from the embedded 3-D CRMs. The ESMT scheme treats both zonal and meridional large-scale momentum as nonconserved scalars, which are advected by resolved fine-scale flows from CRM simulations. Due to the lack of the third dimension in the 2-D CRM, the ESMT scheme implicitly assumes that the spatial structure of the advecting flow field is the same in both horizontal directions. After calculating cloud-scale pressure gradient force at each CRM time step, the momentum feedback is evaluated for both large-scale wind components and implemented at each GCM grid in E3SM. It is worth mentioning that the momentum feedback from the ESMT scheme is calculated diagnostically based on the CRM flows without directly affecting the vertical structure of convective heating. The momentum feedback only affects GCM flows directly through the momentum tendency in

MMF2DMF and MMF3DMF, and vanishes when the momentum feedback option is switched off in MMF2D and MMF3D The implementation is similar to how ESMT was implemented in SP-WRF (Tulich, 2015), except that the CRM orientation in SP-WRF is allowed to vary depending on large-scale horizontal flow. For convenience, all output fields are further remapped onto a 1deg-by-1deg regular grid in pressure coordinates. Global 2-D fields (e.g., precipitation rate) are outputted every 3 hours, while global 3-D fields (e.g., zonal wind) are outputted daily.

2.2 Observational and reanalysis data for comparison

Three observational and reanalysis datasets spanning a 19-year period (2001–2019) are used in this study to compare with model results. The first dataset is the monthly mean and hourly zonal wind in the $0.25^\circ \times 0.25^\circ$ horizontal resolution from the fifth-generation ECMWF reanalysis (ERA5) data product. We further coarse-grain it onto the $1^\circ \times 1^\circ$ grids to match the horizontal resolution of the simulation output. The ERA5 monthly mean zonal wind is used as a reference for observed climatological mean zonal winds in Fig. 2 and 3, while the ERA5 hourly 850hPa zonal wind is used to calculate its observed power spectral density in Fig. 4 and wavenumber-frequency power spectrum in Fig. 6. The second dataset is the monthly mean precipitation rate at $0.1^\circ \times 0.1^\circ$ horizontal resolution from the Integrated Multi-satellitE Retrivals for GPM (IMERG) data product. We also coarse-grain it onto the $1^\circ \times 1^\circ$ grids to match the horizontal resolution of the simulation output. The long-term mean of this IMERG precipitation is used as a reference for the observed climatological mean precipitation rate in Fig. 1. The third dataset is the daily outgoing longwave radiation (OLR) at $2.5^\circ \times 2.5^\circ$ horizontal resolution from the NOAA Interpolated OLR data product. This OLR data is used to calculate the observed wavenumber-frequency power spectrum in Fig. 5.

To extract flow fields associated with the MJO, an MJO reference time series is further obtained by taking the average of OLR over the eastern Indian ocean (80°E–100°E, 10°S–10°N) and using a band-pass filter between 30 and 90 days. All other MJO composite fields are obtained by conducting a lag regression about those fields against the MJO reference time series at each GCM grid.

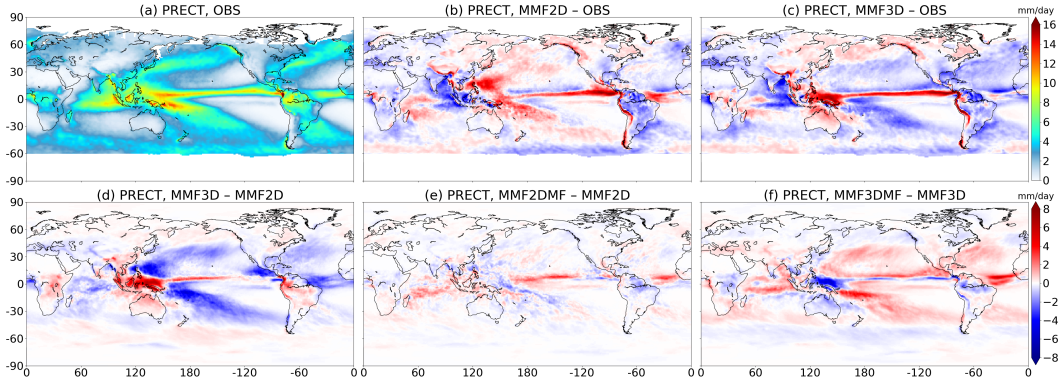

Figure 1. Climatological mean precipitation rate (unit: mm/day) based on (a) 19-year (2001–2019) monthly IMERG data. The remaining panels show the differences of climatological mean precipitation between (b) MMF2D and observation, (c) MMF3D and observation, (d) MMF3D and MMF2D, (e) MMF2DMF and MMF2D, (f) MMF3DMF and MMF3D. Panel (a) uses the top colorbar, while remaining panels use the bottom colorbar. Here MMF2DMF (MMF3DMF) refers to the E3SM-MMF simulations with 2-D (3-D) CRMs and momentum feedback.

3 Impact of convective momentum transport on large-scale circulation and convective organization

The goal of this section is to assess the impact of CMT on model climatology by directly comparing model output from E3SM-MMF simulations with/without momentum feedback. We consider both scenarios with 2-D or 3-D CRMs, and also investigate the impact of the third dimension in the embedded CRMs on the mean state and spatiotemporal variability. We conduct these comparisons in terms of precipitation rate, 850hPa zonal wind, and OLR, and verify the results based on the observational and reanalysis datasets.

3.1 Climatological mean state

Fig. 1 shows the climatological mean precipitation rate averaged over 19-year IMERG satellite data and 10-year E3SM-MMF simulations, respectively. The observation in panel (a) features the large-scale patterns of precipitation including the elongated rainfall belt over the ITCZ, large amounts of rainfall over the warm pool region, and intermediate amounts of rainfall over the subtropical western Pacific and Atlantic oceans in both hemispheres. As shown by panels (b) and (c), both MMF2D and MMF3D exaggerate the precipitation rate over the western Pacific and the ITCZ regions, but underestimate the precipitation over

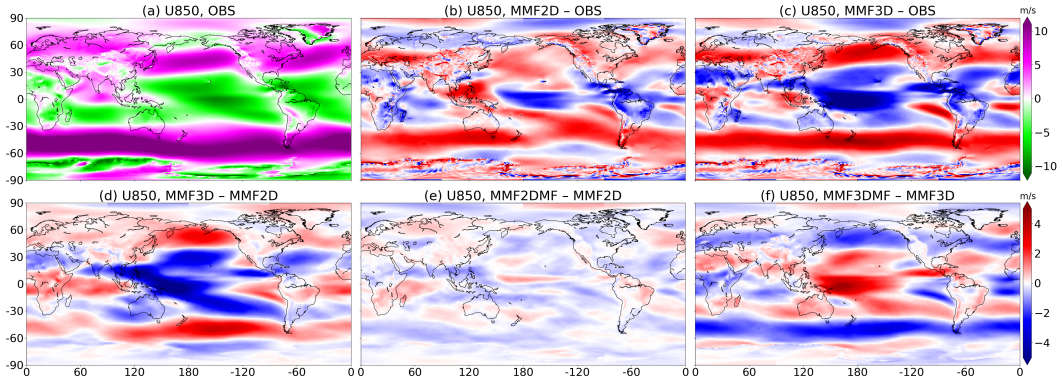

Figure 2. Similar to Fig. 1 but for 850hPa zonal wind (unit: m/s). The climatological mean zonal winds in panel (a) are based on 19-year (2001–2019) monthly mean ERA5 data.

the eastern Indian ocean. Panel (d) reflects the effect of the third dimension in the embedded CRMs in influencing the climatological mean precipitation. Compared with MMF2D, MMF3D is characterized by enhanced precipitation rate over the Maritime continent, the western Pacific, the ITCZ regions, and suppressed precipitation rate over the western Pacific, the western Atlantic and the Indian ocean. Panels (e,f) show the change of mean precipitation rate by enabling momentum feedback in MMF2D and MMF3D, respectively. Both panels feature a mean precipitation decrease over the western Pacific and increases over the ITCZ, the Indian ocean and the subtropical Pacific ocean in both hemispheres, reflecting the general impact of CMT on climatological mean state. However, the changes of mean precipitation due to momentum feedback in panel (e) are weaker than those in panel (f), reflecting the fundamental differences in the way that convection-circulation coupling is simulated in MMFs with embedded 2-D vs. 3-D CRMs.

Fig. 2 shows the climatological mean zonal winds at 850 hPa. The observation in panel (a) features the distribution of 850-hPa zonal winds with equatorial easterlies and mid-latitude westerlies. Specifically, these westerlies over the Indian ocean and Maritime continent and easterlies over the Pacific belong to the lower branches of the Walker circulation. As shown by panels (b) and (c), both MMF2D and MMF3D exaggerate this zonal wind distribution with the bias in a similar pattern. The equatorial easterly bias over the Pacific in panel (c) is stronger than those in panel (b), indicating stronger low-level moisture convergence over the western Pacific and explaining the enhanced precipitation rate over that region in Fig. 1c. As shown by panel (d), compared with MMF2D, MMF3D has

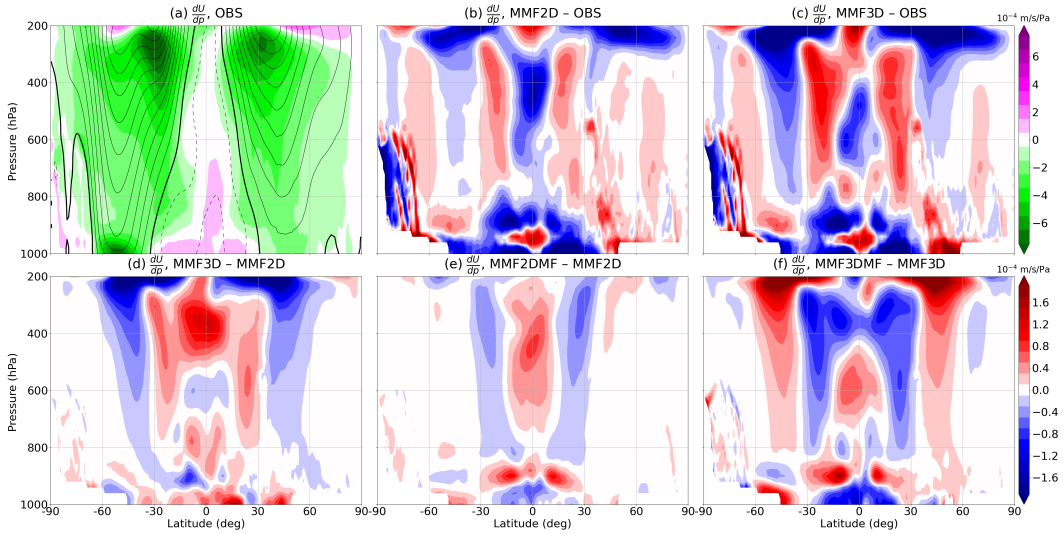

Figure 3. Similar to Fig. 1 but for vertical gradient of zonal wind in pressure coordinates (unit: 10^{-4} $m/s/Pa$). The solid and dashed contours (contour interval 3 m/s) in panel (a) indicates the climatological mean westerlies and easterlies, respectively.

enhanced equatorial easterlies over the Pacific and mid-latitude westerlies in both hemispheres. Panels (e,f) show the change of mean zonal winds by enabling momentum feedback in MMF2D and MMF3D, respectively. In panel (e), westerly anomalies prevail over the central Pacific, the western Indian ocean, and several subtropical regions, while easterly anomalies prevail in the remaining regions. The spatial pattern of mean wind change due to momentum feedback is similar to the climatological zonal wind bias in panel (b) but in an opposite sign, indicating the cumulus friction effects due to CMT. The mean zonal wind change in panel (e) is similar to that in panel (f) but with a much weaker magnitude, again reflecting the fundamental differences in the way that convection-circulation coupling is simulated in MMFs with embedded 2-D vs. 3-D CRMs.

Vertical wind shear plays an important role in initiating convective activities and its organization. Fig. 3 shows the climatological zonal mean vertical shear of zonal winds. The observation in panel (a) features a positive lower-tropospheric wind shear near the equator and negative ones throughout the whole troposphere at mid-latitudes. Both MMF2D and MMF3D in panels (b) and (c) exaggerate the lower-tropospheric wind shear near the equator but underestimate its magnitude in the neighboring levels. They also feature negative wind shear bias over the subtropical regions but positive biases at mid-latitudes. As shown by panel (d), compared with MMF2D, MMF3D features enhanced positive wind shear near the

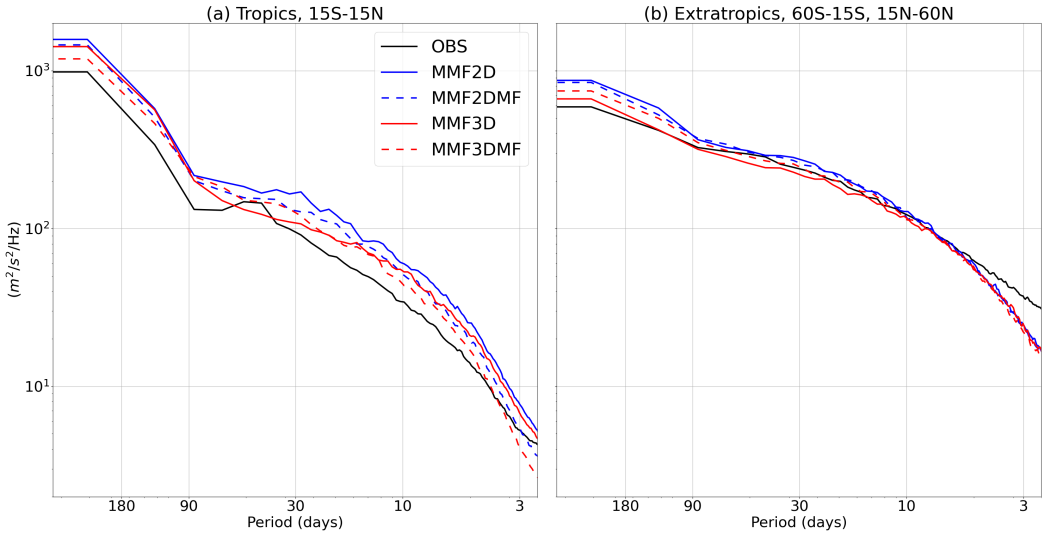

Figure 4. Power spectral density of 850hPa zonal winds averaged over (a) tropics (15°S–15°N), and (b) extratropics (60°S–15°S, 15°N–60°N). In each panel, the black curve is based on 19-year (2001–2019) ERA5 hourly data, while the blue solid, blue dashed, red solid, red dashed curves are based on 10-year MMF2D, MMF2DMF, MMF3D, MMF3DMF simulations, respectively.

equator and negative one at mid-latitudes, consistent to the overall enhanced mean precipitation and circulation in Fig. 1 and 2. In panel (e), the change of wind shear near the equator is characterized by positive anomalies above 900 hPa and negative anomalies below that level, further lifting the peak of wind shear upward. In contrast, the change of wind shear features negative wind shear in the subtropical regions and positive one at mid-latitudes, promoting the equatorial displacement of the peak of wind shear. Such changes are similar to those concluded in other studies (Wu & Yanai, 1994; Richardson et al., 2007; Rappin & Nolan, 2012) that the vertical shear plays an important role for convective organization mechanisms (e.g., cold pool dynamics and moisture-stratiform instability). Compared with panel (e), panel (f) shows a similar pattern of vertical wind shear change but with a much stronger magnitude, reflecting the difference between MMF2DMF with the ESMT scheme and MMF3DMF featuring 3-D flows in estimating the magnitude of CMT.

3.2 Variability of 850hPa zonal winds at different time scales

Fig. 4 shows the power spectral density of zonal winds at 850 hPa based on the 19-year ERA5 data and 10-year E3SM-MMF simulations. As shown by panel (a) for the tropics, both MMF2D and MMF3D overestimate the power spectral density in all timescales. Com-

pared with MMF2D (solid blue curve), MMF3D (solid red curve) has reduced variability of 850hPa zonal winds on the intraseasonal time scale between 10 and 90 days, closer to the observation, but similar variability in the remaining period as MMF2D. When enabling momentum feedback, MMF2DMF (dashed blue curve) features reduced variability for periods shorter than 90 days, indicating the important role of CMT in controlling intraseasonal and high-frequency wave activities. In contrast, MMF3DMF (dashed red curve) has reduced variability for periods shorter than 30 days and longer than 90 days, but enhanced variability for periods between 30 and 90 days. The different effects of CMT in MMF2DMF and MMF3DMF on intraseasonal variability of zonal winds reflect its complex interactions with the large-scale circulation, presumably due to the different background state and its variability in the MMF2D and MMF3D simulations. Since the behavior of MMF3D is vastly different from MMF2D, the effects of CMT in the two cases are not expected to be the same. For the extratropics in panel (b), the differences among the four E3SM-MMF simulations are much smaller. Overall, all four cases overestimate the power spectral density for periods longer than 5 days, but underestimate that for periods shorter than 5 days. Unlike the major changes for periods shorter than 90 days in the tropics (panel a), both MMF2DMF and MMF3DMF feature major changes for periods longer than 90 days in the extratropics (panel b), reflecting the contrasting impact mechanisms of CMT on wave activities over the tropics and extra-tropics.

3.3 Spatiotemporal variability of tropical convection

Fig. 5 shows the normalized wavenumber-frequency power spectra of the meridionally symmetric component of OLR based on the 19-year NOAA Interpolated OLR data and 10-year E3SM-MMF simulations. Both MMF2D in panel (b) and MMF3D in panel (c) reproduce the observed large-scale tropical wave modes in panel (a), including the MJO, Kelvin waves and Rossby waves. Unlike the observed dominant MJO in wavenumber 1-4, the spectrum peak of MJO mode in panels (b,c) is mostly confined to wavenumber 1-2 in a much weaker magnitude. In contrast, both MMF2D and MMF3D have stronger power spectrum of Kelvin waves and Rossby waves than the observation. MMF2D features significant power spectrum of the westward-moving tropical depression mode (Wheeler & Kiladis, 1999), while that in MMF3D is even as strong as the Kelvin waves but in the opposite propagation directions. Such dominant westward-propagating mode is also found in the previous E3SM-MMF simulations (see Figure 8 in W. M. Hannah et al. (2020)). The differences between

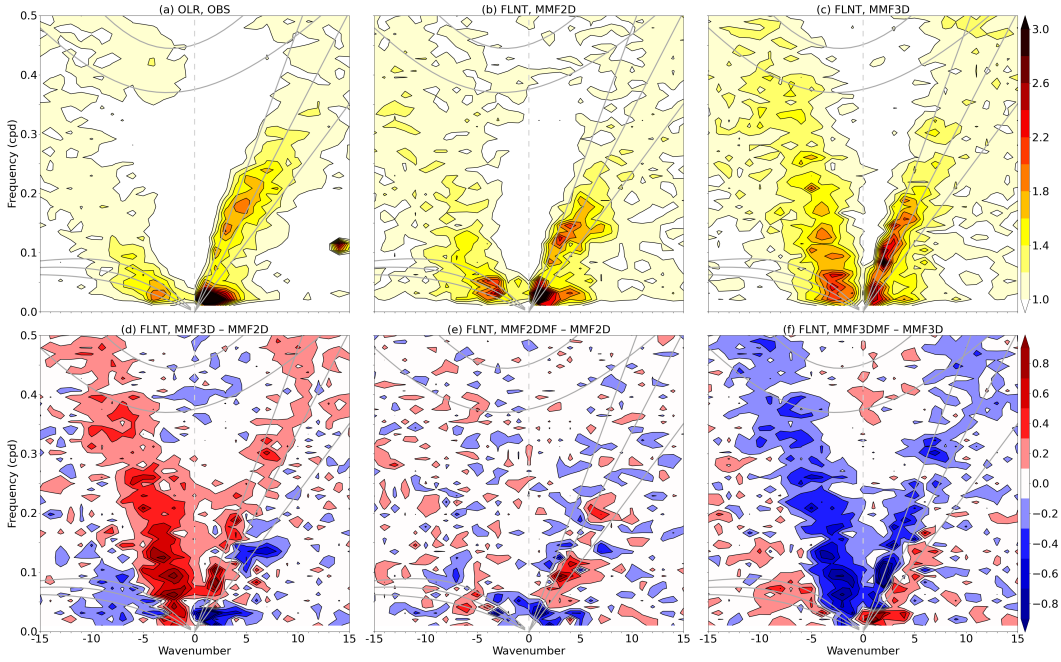

Figure 5. Normalized wavenumber-frequency power spectra of the meridionally symmetric component of (a) 19-year (2001–2019) NOAA Interpolated daily OLR (unit: W/m^2), (b) 10-year MMF2D daily net longwave flux at top of model (FLNT, unit: W/m^2), (c) 10-year MMF3D daily FLNT. Panels in the second row show the difference of FLNT power spectrum between (d) MMF3D and MMF2D, (e) MMF2DMF and MMF2D, (f) MMF3DMF and MMF3D. These power spectra are calculated as the ratio between the raw spectra and smoothed background spectra for normalization, and thus their differences should highlight changes to the relative power distribution.

MMF2D and MMF3D in simulating convectively coupled equatorial waves can be partly attributed to the different structures of background zonal flows. The recent study by Tulich and Kiladis (2021) documented a profound sensitivity of both Kelvin waves and the MJO to the structure of the background zonal flow. Besides the large differences of 850hPa zonal flow as shown in Fig. 2d, a further investigation (not shown) indicates that the simulated climatological 200hPa zonal winds are enhanced in MMF3D than MMF2D. As shown by panel (d), compared with MMF2D, MMF3D features reduced power spectrum of the MJO mode but enhanced power spectrum of Kelvin and Rossby waves, a faster phase speed of Kelvin waves, and the dominant westward-moving easterly waves. When enabling the momentum feedback, MMF2DMF in panel (e) features reduced power spectrum of the MJO mode but enhanced one of the Kelvin waves, while MMF3DMF in panel (f) features a similar pattern but in an opposite sign. This opposite effect of CMT on the MJO mode is consistent with the power spectral density change on the intraseasonal time scale in Fig. 4a. MMF3DMF also exhibits reduced power spectrum of the dominant easterly waves and a slower phase speed of Kelvin waves, resembling the observation. It is worth noting that the CMT induced power spectrum changes in panel (f) are similar to those in panel (d), indicating that CMT helps to reduce model biases found in MMF3DMF and reflecting its crucial role in capturing realistic large-scale circulation and convective organization.

Fig. 6 shows the normalized wavenumber-frequency power spectra of the meridionally symmetric component of zonal winds at 850 hPa based on the 19-year ERA5 data and 10-year E3SM-MMF simulations. Similar to the observed power spectrum in panel (a), both MMF2D in panel (b) and MMF3D in panel (c) capture the dominant MJO mode, Kelvin and Rossby waves, as well as westward-moving easterly waves. That said, both MMF2D and MMF3D underestimate the power spectrum of the MJO mode. Also, Kelvin waves in both cases are much more confined to larger wavenumbers 1-5, while those in the observation are in wavenumbers 1-10. As shown by panel (d), compared with MMF2D, MMF3D has reduced power spectrum of the MJO mode, enhanced power spectrum of Kelvin and Rossby waves, and higher frequency of easterly waves. When enabling the momentum feedback, MMF2DMF in panel (e) features reduced power spectrum of the MJO mode and enhanced power spectrum of Kelvin waves, while MMF3DMF in panel (f) features a similar pattern but in an opposite sign. These opposite effects of CMT on the MJO and Kelvin waves in MMF2DMF and MMF3DMF are consistent with Fig. 5e-f. MMF3DMF has reduced power spectrum of easterly waves due to the presence of CMT, and resembles the observation data.

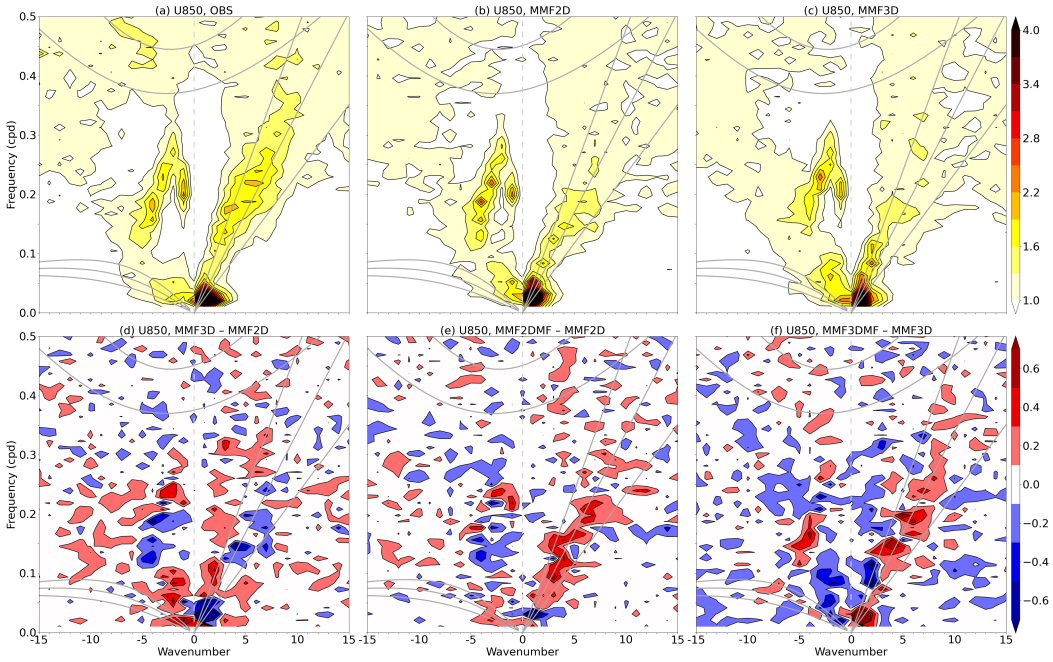

Figure 6. Similar to Fig. 5 but for 850hPa zonal winds (unit: m/s).

4 Representation of convective momentum transport through the ESMT scheme

The goal of this section is to verify the skill of the ESMT scheme in reproducing CMT in MMF2DMF relative to CMT that is explicitly resolved in MMF3DMF. The tendencies from CMT consist of two components, the zonal and meridional components, in the horizontal plane. It is worth mentioning that the ESMT scheme in MMF2DMF is based on flows from the embedded 2-D CRMs that are orientated in the north-south direction. The implicit assumption that the spatial structure of the advecting flow field is the same in both horizontal directions is used to calculate the parameterized pressure gradient force in the ESMT scheme (Tulich, 2015). In contrast, CMT in MMF3DMF is directly calculated by using the embedded 3-D CRM flows. The fairness of the direct comparison of CMT between MMF2DMF and MMF3DMF is based on the assumption that the background mean state is similar in MMF2D and MMF3D. That said, it is worth noting that the background mean states in MMF2DMF and MMF3DMF are different from one another in a few ways, as shown in Figs. 1d, 2d, and 3d. Without loss of generality, we mainly focus on the zonal component of CMT in the following comparisons. In this study, we refer to the kinetic forcing from the GCM to the CRM as momentum forcing, and refer to the momentum tendency from the CRM to the GCM as momentum feedback.

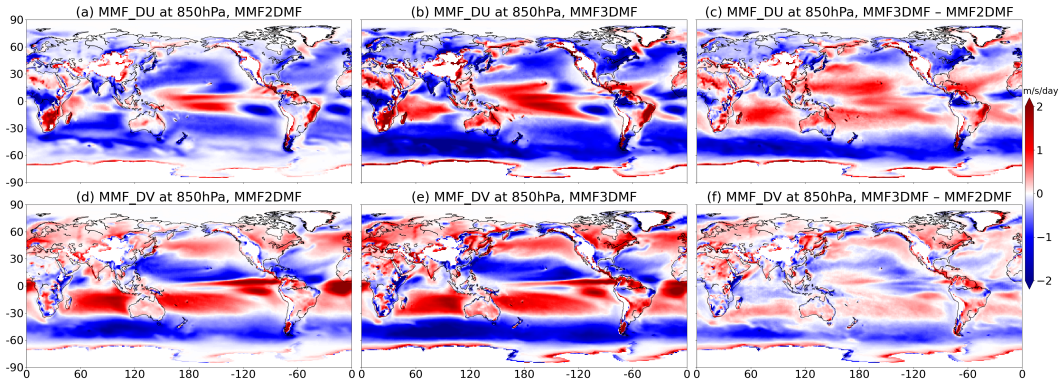

Figure 7. Climatological mean horizontal profiles of zonal component of momentum feedback MMF_DU (unit: $m/s/day$) at 850hPa from (a) MMF2DMF, and (b) MMF3DMF. Panel (c) shows their difference. Panels (d-f) are similar to panels (a-c) but for meridional component of momentum feedback MMF_DV at 850hPa.

4.1 Climatological mean state of convective momentum transport

Fig. 7 shows the climatological mean 850hPa horizontal distributions of CMT in MMF2DMF and MMF3DMF. For its zonal component, both panels (a) and (b) feature eastward momentum feedback over the central Pacific, the Indian ocean, and subtropical continental regions, and westward momentum feedback at mid-latitudes in both hemispheres. This momentum feedback has opposite signs as those in Fig. 2, decelerating both equatorial easterlies and mid-latitude westerlies and reflecting its cumulus friction effect on climatological mean circulation. In spite of their similar spatial patterns, the momentum feedback in MMF2DMF is much weaker than that in MMF3DMF in both the tropics and mid-latitudes. The difference of the momentum feedback in panel (c) has the same magnitude as the total momentum feedback, presumably due to the different magnitudes of the vertical shear, as shown by Fig. 3b-c. As for the meridional component of CMT, both panels (d) and (e) share a similar spatial pattern with equatorial momentum feedback convergence over the western and central Pacific, northward momentum feedback over the eastern Pacific, the southern Indian ocean, and equatorial Atlantic ocean, and strong southward momentum feedback over the mid-latitude southern hemisphere. Their difference in panel (f) has a much weaker magnitude than that in panel (c), presumably due to the north-south oriented CRMs with directly resolved 2-D flows in MMF2DMF. That said, it is also possible that the smaller differences in the meridional component of CMT is due to the weaker differences in vertical shear of meridional winds between MMF2D and MMF3D.

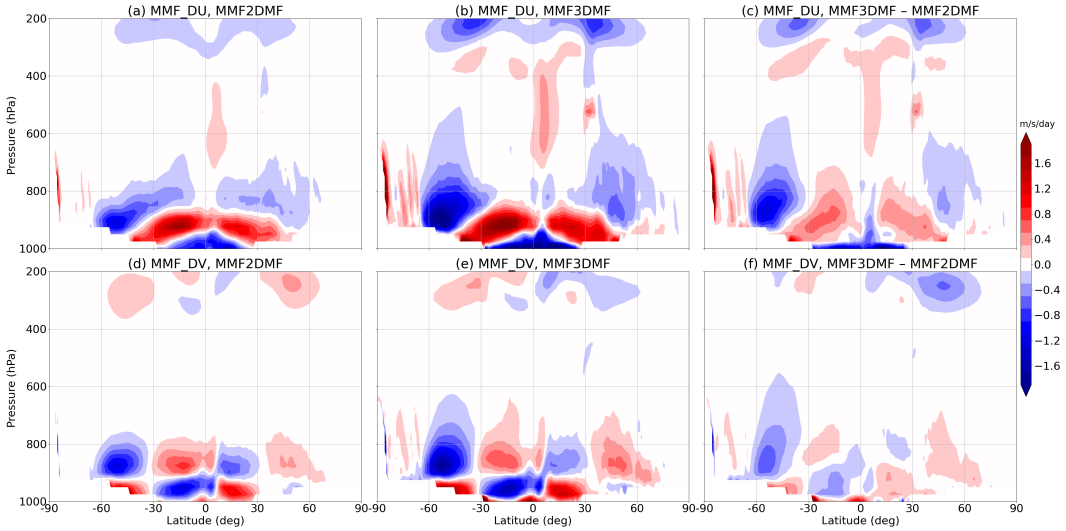

Figure 8. Similar to Fig. 7 but for climatological zonal mean vertical profiles of MMF_DU and MMF_DV.

Fig. 8 shows the climatological zonal mean vertical profiles of CMT in MMF2DMF and MMF3DMF. For its zonal component, both panels (a) and (b) share a similar spatial pattern of momentum feedback with the most significant anomalies confined below the level 800 hPa and only weak positive anomalies above that level. In the tropical regions (30°S–30°N), eastward momentum feedback prevails at levels between 800 hPa and 900 hPa, while westward momentum feedback dominates below 900 hPa. Strong westward momentum feedback is also found at mid-latitudes in the southern hemisphere, decelerating the westerly jets as shown in Fig. 2b-c. However, the magnitude of momentum feedback in panel (a) is weaker than that in panel (b), resulting in a large differences in panel (c). As for the meridional component of CMT, both panels (d) and (e) are characterized by the most significant anomalies at levels below 800 hPa with dipoles of momentum feedback in the tropical regions and mid-latitudes. Their differences in panel (f) have a much weaker magnitude than that in panel (c), reflecting a better skill of the ESMT scheme in capturing the meridional component of CMT than its zonal component.

4.2 Spatiotemporal variability of convective momentum transport

Besides the climatological mean state, it is also important to investigate how well the spatiotemporal variability of CMT is reproduced by the ESMT scheme in MMF2DMF in comparison with that in MMF3DMF. Fig. 9 shows the horizontal distributions of standard

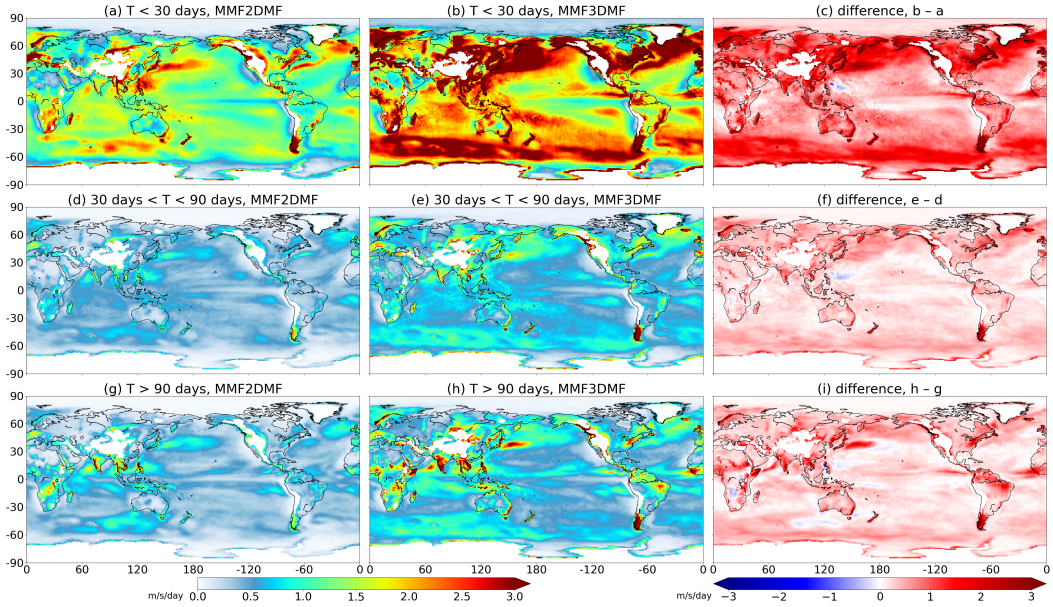

Figure 9. Horizontal profiles of standard deviation of MMF_DU (unit: $m/s/day$) at 850 hPa from (a) MMF2DMF, and (b) MMF3DMF. Panel (c) shows their difference. In each column, panels from top to bottom correspond to filtered solution in a period of (a) $T \leq 30$ $days$, (b) 30 $days < T < 90$ $days$, (c) $T \geq 90$ $days$.

deviation of CMT in MMF2DMF and MMF3DMF. Overall, MMF2DMF and MMF3DMF share a similar spatial pattern of spatiotemporal variability of CMT, including high frequency variability (less than 30 days), intraseasonal variability (between 30 and 90 days), and seasonal variability (longer than 90 days). For the high frequency variability in panels (a-b), the most significant variability is confined to the mid-latitudes of both hemispheres, presumably related to the mid-latitude synoptic-scale systems. Panel (c) shows the difference of high frequency variability between MMF3DMF and MMF2DMF with positive anomalies all over the globe, demonstrating the stronger variability of CMT in MMF3DMF. It should be an interesting future research direction to investigate the relevance of high-frequency CMT variability to the high-frequency precipitation variability. For intraseasonal variability in panels (d,e), both MMF2DMF and MMF3DMF also feature significant variability over the warm pool region and southern Asian monsoon region, presumably due to the prevailing MJO and boreal summer intraseasonal oscillation (BSISO) events. The difference map in panel (f) also reflects the stronger intraseasonal variability of CMT in MMF3DMF. For seasonal variability in panels (g,h), MMF2DMF and MMF3DMF are further characterized by significant variability in the tropical regions, which is associated with

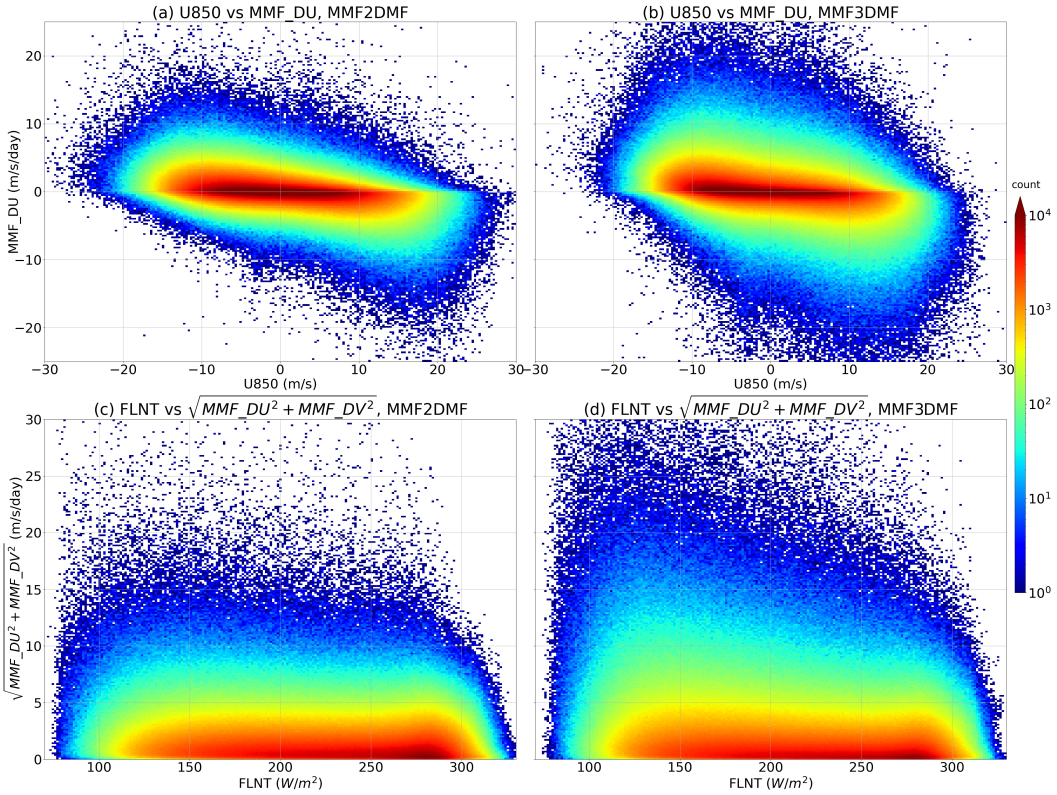

Figure 10. 2-D histogram for zonal wind and MMF_DU at 850 hPa over the warm pool region (60°E–170°E, 10°S–10°N) from (a) MMF2DMF and (b) MMF3DMF. Panels (c,d) are similar to panels (a,b) but for FLNT and strength of momentum feedback at at 850 hPa.

the seasonal migration of the ITCZ region. Their difference map in panel (i) is similar to panel (f). To be brief, the ESMT scheme readily captures the spatial pattern of CMT on high-frequency, intraseasonal, and seasonal time scales. That said, the magnitude of CMT in MMF2DMF is much weaker than that in MMF3DMF.

In general, CMT due to convective scale turbulent flows in the embedded CRMs is coupled to large-scale circulation resolved on the GCM grids. It is important to investigate the relation between CMT and large-scale environmental conditions and verify how such a relation is represented in the ESMT scheme. Fig. 10 shows the 2-D histogram for the zonal component of CMT and zonal winds at 850 hPa as well as OLR. In panels (a,b), both MMF2DMF and MMF3DMF feature a negative correlation between 850hPa zonal winds and the zonal component of CMT. That is, CMT induces westward (eastward) momentum feedback in the presence of lower-tropospheric background westerlies (easterlies). This result is consistent with the theoretical studies by Yang and Majda (2017, 2018, 2019);

Yang, Majda, and Moncrieff (2019), stating that downshear-propagating MCSs in a front-to-rear tilting structure induce eastward (westward) momentum feedback in the presence of lower-tropospheric background westerlies (easterlies). However, MMF2DMF in panel (a) is characterized by a narrower distribution spread of CMT in the presence of large zonal winds than MMF3DMF in panel (b), reflecting less moderation effect of CMT by background zonal winds in the ESMT scheme. Such differences between MMF2DMF and MMF3DMF may also be related to the differences of the background vertical shear. Panels (c,d) show the 2-D histogram for CMT strength and OLR. In particular, MMF3DMF in panel (d) features a wider distribution spread of CMT strength in the presence of lower OLR, indicating the fact that CMT becomes much stronger due to enhanced turbulent flows and convective activities in the embedded CRMs. However, such a feature is less significant in MMF2DMF in panel (c) with a uniformly distributed spread of CMT strength, reflecting the fundamental differences in the way that convection-circulation coupling is simulated in MMFs with embedded 2-D vs. 3-D CRMs.

4.3 Zonal momentum budget over the eastern Indian ocean

CMT plays an important role in the momentum budget associated with large-scale circulation and convective organization, which was concluded by both observational studies (e.g., Tung & Yanai, 2002a) and numerical simulations (e.g., Grabowski & Moncrieff, 2001). Fig. 11 shows the vertical profiles of zonal momentum budget terms over the eastern Indian ocean based on the 10-year E3SM-MMF simulations. For the climatological mean vertical profiles, both MMF2DMF and MMF3DMF feature a dominant balance between dynamical zonal wind term in panels (b,f) and zonal component of CMT term in panels (c,g). The vertical diffusion and gravity wave drag terms in panels (d,h) only have some impact at levels below 800 hPa, and the total time tendency term in panels (a,e) is negligible over the long-term mean. The ESMT scheme readily captures the climatological mean vertical profiles of all momentum budget terms but underestimate their magnitude in both lower and upper troposphers, particularly for the dynamical zonal wind term in panel (b) and the zonal component of CMT term in panel (c). As for their variability, MMF2DMF shows a similar vertical distribution of standard deviation of total time tendency in panels (a,e), dynamical zonal wind term in panels (b,f), and vertical diffusion and gravity wave drag term in panels (d,h) as MMF3DMF. However, the variability of CMT in panel (c) at levels between 800 and 200 hPa is much weaker than that in panel (g). The fact that the dynamical

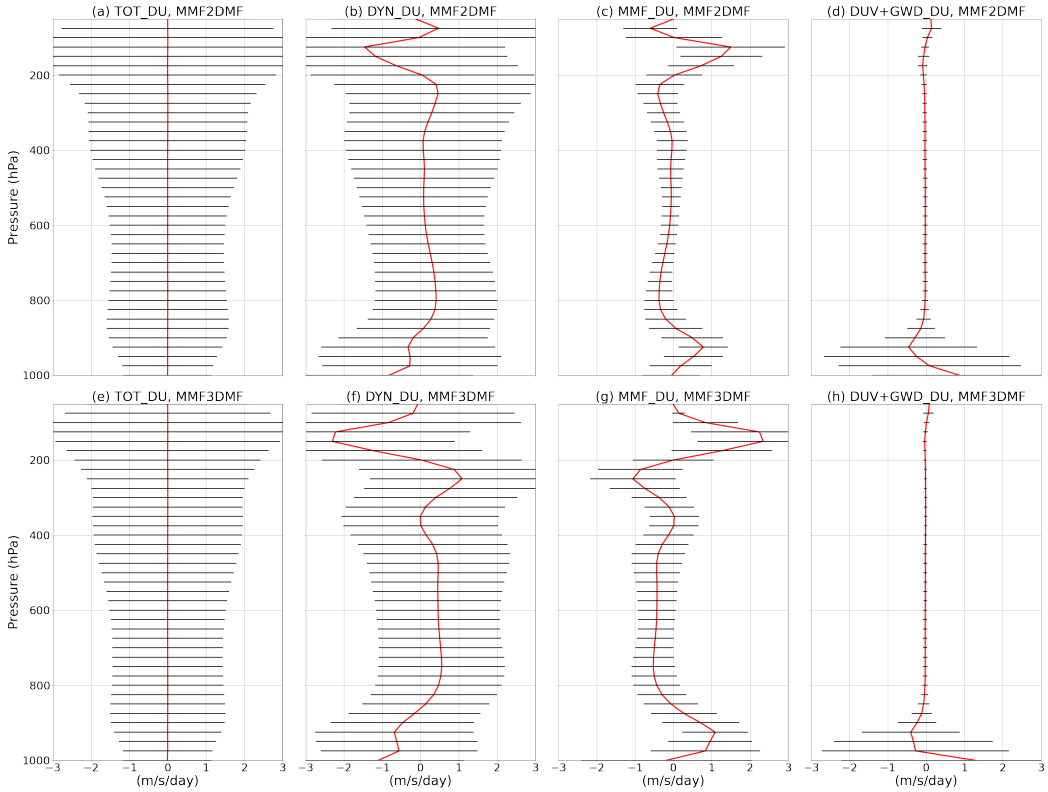

Figure 11. Vertical profiles of zonal momentum budget terms over the eastern Indian ocean (80°E–100°E, 10°S–10°N) from the MMF2DMF simulation, including (a) total zonal wind tendency term TOT_DU, (b) dynamics zonal wind term DYN_DU, (c) momentum feedback term MMF_DU, and (d) vertical diffusion and gravity wave drag term DUV+GWD_DU. In each panel, the red curve corresponds to the mean at a specific level and horizontal line indicates one standard deviation from the mean. Panels (e-h) are similar to panels (a-d) but from the MMF3DMF simulation.

zonal wind term in MMF2DMF (panel b) is weaker than that in MMF3DMF (panel f) and balanced by a weaker CMT in panel (c) implies that the differences in CMT could also stem from fundamental differences between the behaviors of MMF2D and MMF3D.

This momentum budget analysis reflects the important role of CMT in maintaining mean circulation and its variability over this region, where large-scale convective organizations such as the MJO typically prevail. In particular, the CMT with lower-tropospheric eastward momentum feedback and and upper-tropospheric westward momentum feedback has the same sign as both the background zonal winds and the MJO wind fields, thus accelerating the large-scale zonal winds. This is consistent with the conclusion of Brenowitz et al. (2018); Yang, Majda, and Brenowitz (2019) that the CMT promotes planetary-scale organization of convection by serving as the dominant kinetic energy source.

5 Impact of convective momentum transport on the Madden-Julian Oscillation

The goal of this section is to investigate the impact of CMT on the MJO propagation and vertical structure and further verify the representation of CMT in MMF2DMF in comparison with MMF3DMF.

5.1 Characteristic features of MJO propagation

Fig. 12 shows the longitude-time diagram for MJO composite of various fields in MMF2DMF and MMF3DMF. As shown by panels (a,b), both MMF2DMF and MMF3DMF feature the eastward propagation of a planetary-scale MJO precipitating event accompanied by zonal wind convergence in the lower troposphere. However, the precipitation rate in panel (a) reaches the maximum at longitude 90°E and 150°E and exhibits weak magnitude between these two regions, resembling the observed barrier effect of the Maritime continent on the MJO propagation (C. Zhang & Ling, 2017). In contrast, MMF3DMF in panel (b) features a persistent eastward-propagating precipitation event with slightly stronger wind convergence in the lower troposphere, presumably due to the additional dimension in the embedded CRMs with enhanced convective activities. Panels (c,d) further show the longitude-time diagram for the zonal component of CMT on top of the 850hPa zonal winds. Both MMF2DMF and MMF3DMF capture the negative correlation between background zonal winds and the zonal component of CMT, that is, eastward (westward) momentum feedback overlaps with easterlies (westerlies), reflecting the overall damping effect of CMT

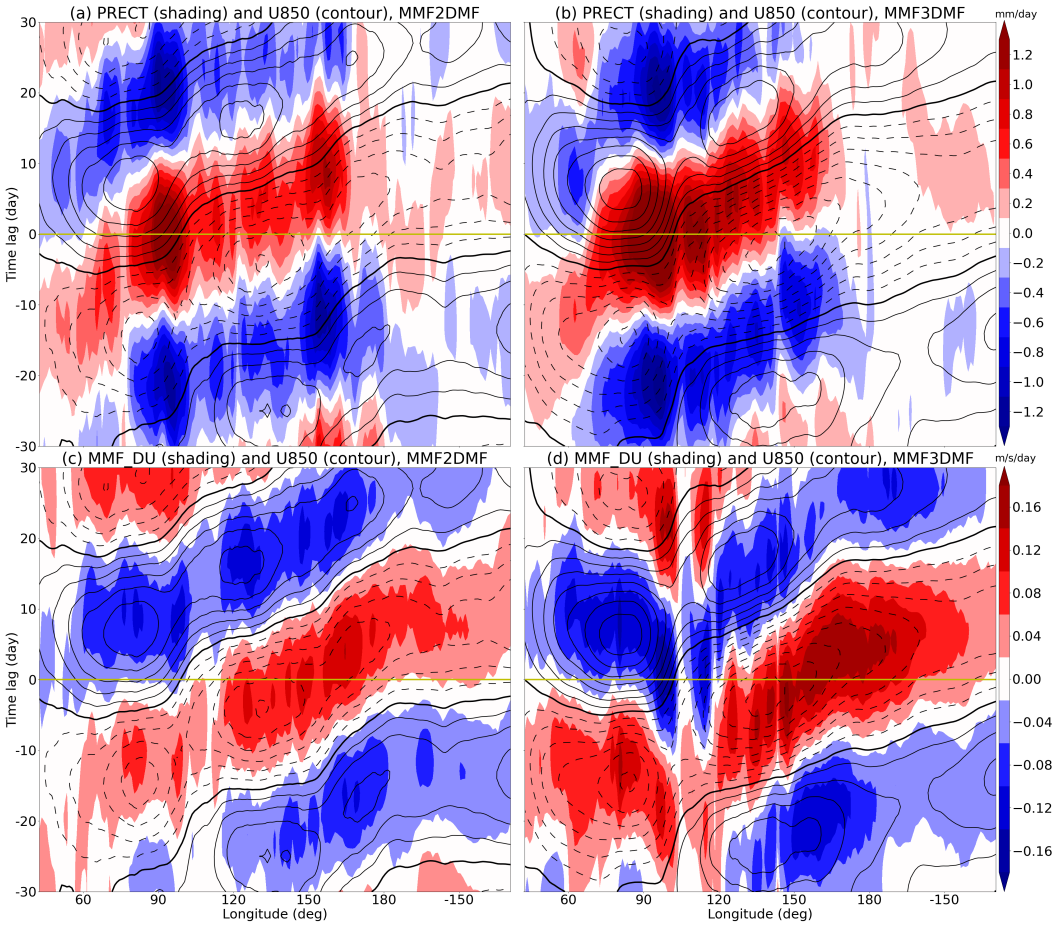

Figure 12. Longitude-time MJO composite of various fields based on lag-regression against 30–90 days filtered FLNT time series averaged over the eastern Indian ocean (80°E–100°E, 10°S–10°N). Panel (a) shows 850hPa zonal wind (contours, interval 0.15 m/s) and precipitation rate (shading, unit: mm/day) from the MMF2DMF simulation, while panel (b) is from the MMF3DMF simulation. Panels (c,d) are similar to panels (a,b) but for 850hPa zonal wind (contours, interval 0.15 m/s) and MMF_DU (shading, unit: $m/s/day$). The horizontal yellow line indicates the lag 0.

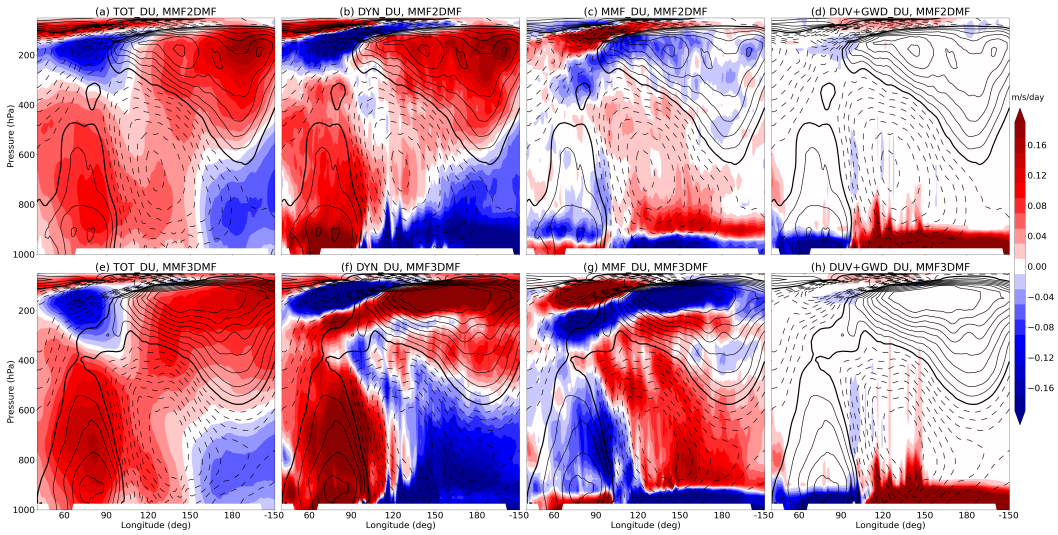

Figure 13. Longitude-height MJO composite of zonal momentum budget terms (shading, unit: $m/s/day$) and zonal wind (contours, interval 0.15 m/s) based on lag regression against 30–90 days filtered FLNT time series averaged over the eastern Indian ocean (80°E–100°E, 10°S–10°N) from the MMF2DMF simulation, including (a) total zonal wind tendency term TOT_DU, (b) dynamical zonal wind term DYN_DU, (c) momentum feedback term MMF_DU, and (d) vertical diffusion and gravity wave drag term DUV+GWD_DU. Panels (e-h) are similar to panels (a-d) but from the MMF3DMF simulation.

on large-scale circulation. Both cases feature a discontinuity of CMT over the regions at longitude 110°E, presumably due to the topography effect over the Maritime continent. That said, the magnitude of CMT in panel (c) is much weaker than that in panel (d), presumably due to the different strength of background wind shear and convective activities in MMF2DMF and MMF3DMF.

5.2 Acceleration and deceleration effects of convective momentum transport on the MJO

The momentum budget analysis is a useful tool for understanding the underlying dynamical mechanisms associated with the MJO, providing a benchmark for testing the prediction skills of GCMs in simulating large-scale convective organization(Oh, Jiang, Waliser, Moncrieff, Johnson, & Ciesielski, 2015). Fig. 13 shows the longitude-height diagram for MJO composite of zonal momentum budget terms and zonal winds in MMF2DMF and MMF3DMF. As for zonal winds, both MMF2DMF in panels (a-d) and MMF3DMF in

panels (e-h) capture the vertical profile of MJO zonal winds with lower-tropospheric wind convergence and upper-tropospheric wind divergence in a front-to-rear tilting structure. In particular, the lower-tropospheric inflows at the leading edge and near-surface westerlies at the trailing edge in MMF3DMF are slightly stronger than those in MMF2DMF, consistent with the stronger precipitation rate in Fig. 12b and 12d. As for the total time tendency of zonal momentum in panels (a,e), both cases are characterized by a similar pattern of time tendency as zonal wind but displaced eastward by tens of degree, consistent with the eastward propagation of the MJO. The vertical profiles of dynamical zonal wind term in panels (b,f) are quite similar to that of the total time tendency, reflecting the dominant contribution of the dynamical zonal wind processes (advection effect, Coriolis force, and pressure gradient force) to the eastward propagation of the MJO. As for the zonal component of CMT in panels (c,g), both cases feature alternating zonal momentum feedback with convergence near the surface and divergence above the 900 hPa level, accelerating the near-surface easterlies (westerlies) at the leading (trailing) edge of the MJO but decelerating those flows above. However, this decelerating effect due to CMT further extends to the middle and upper troposphere in panel (g), while that in panel (c) is almost negligible. The weak magnitude of CMT in MMF2DMF is consistent with its small variability in the middle troposphere, as shown in Fig. 11c. It is also possible that the differences in CMT are due to the stronger MJO convective signals over the Maritime Continent in MMF3DMF than MMF2DMF, as shown in Fig. 12. CMT in both cases also induce deceleration effects on the upper-tropospheric wind divergence in an eastward tilting structure in height, presumably related to propagating gravity waves excited by the MJO convective activities. The discrepancies in these spatial patterns between MMF2DMF and MMF3DMF reflect the fundamental differences in the way that convection-circulation coupling is simulated in MMFs with embedded 2-D vs. 3-D CRMs. Lastly, both cases exhibit a similar pattern of vertical diffusion and gravity wave drag term with the most significant anomalies confined near the surface, which cancel out with the zonal wind tendencies from dynamics.

6 Discussion and conclusion

For E3SM-MMF, 2-D CRMs are embedded in each GCM grid to simulate subgrid-scale flows and convective activities. Due to the lack of the third dimension, these 2-D CRMs provide small-scale turbulent flows along only one horizontal direction that are not sufficient to calculate the zonal and meridional components of CMT. In order to represent CMT in

E3SM-MMF with a 2-D CRM, we employ the ESMT scheme of Tulich (2015) to achieve the full coupling of momentum budget between GCM and CRM resolved flows. We first investigate the impact of CMT on climatological mean state and spatiotemporal variability of large-scale circulation and tropical convection in comparison with the observation, and then verify the skill of the ESMT method in representing CMT by comparing results between E3SM-MMF with 2-D and 3-D CRMs, in which CMT is parameterized and explicitly resolved, respectively. Finally, we discuss the impact of CMT on the MJO propagation and vertical structure.

By comparing the model output from E3SM-MMF simulations with/without momentum feedback, we infer the impact of CMT on large-scale circulation and convective organization. Unlike the CMT in MMF2DMF that is represented through the ESMT scheme, the CMT in MMF3DMF is directly calculated based on the turbulent flows resolved by the embedded CRMs and used as a reference for comparison. The results show that CMT helps reduce precipitation bias over the western Pacific and the ITCZ regions in Fig. 1e-f, which is associated with the reduced easterlies over the Pacific in Fig. 2e-f, weakening the low-level moisture convergence and thus convective activities over the western Pacific. In fact, Tulich (2015) conducted a series of seasonal global integration of the SP-WRF and also concluded that the inclusion of momentum feedback through the ESMT scheme helps to reduce model bias in mean precipitation over the equatorial western Pacific, the ITCZ, and the Indian monsoon regions (see its Figure 11b). Similar results were also reported in other studies based on different CMT parameterizations. For example, Cheng and Xu (2014) added a mass flux based CMT parameterization in their MMF simulation and improved the spatial distribution, amplitude, and intraseasonal variability of the surface precipitation in the tropics (see its Figure 1). Such a drying effect due to CMT was also concluded by Moncrieff et al. (2017) where a parameterization of CMT based on slantwise coherent structure of MCSs was added to the NCAR Community Atmosphere Model (CAM), which reduced significantly the model bias in mean precipitation over the western Pacific (see its Figure 14a). Our results also show that CMT helps reduce the lower-tropospheric vertical wind shear in the tropics and upper-tropospheric vertical wind shear at mid-latitudes in Fig. 3e-f. This reduced vertical wind shear due to CMT is consistent with the conclusion by Woelfle et al. (2018) about the inadequate vertical mixing of zonal momentum from the absence of CMT in SP-CAM. All the results discussed above highlight the crucial role of CMT in influencing the large-scale circulation and provide potential explanations for common model biases in

GCMs. However, the changes of mean precipitation and zonal winds in MMF2DMF are weaker than those in MMF3DMF. Also, the mean precipitation rate in MMF3D in Fig. 1c is stronger than that in MMF2D, indicating the differences between 2-D and 3-D CRMs in simulating convection and the need for further model tuning.

Besides, CMT in both MMF2DMF and MMF3DMF reduces the overall variability of 850hPa zonal winds in Fig. 4a, reflecting its damping effects on large-scale circulation. For tropical waves, CMT in both cases share a similar impact on Kelvin waves with reduced power spectrum and slowdown of phase speed in Fig. 5e-f and 6d-f, better resembling the observation (Kiladis et al., 2009). In contrast, CMT in both cases has opposite impacts on the MJO mode by reducing its spectral power in MMF2DMF but enhancing it in MMF3DMF, consistent with their opposite impacts on the intraseasonal variability of 850hPa zonal winds in Fig. 4a. Such contrasting results are presumably related to the differences between MMF2DMF and MMF3DMF in simulating convective organization, as the MJO mode is largely underestimated in MMF3DMF in Fig. 5c. Moncrieff et al. (2017); Moncrieff (2019) concluded that the incorporation of CMT parameterization in CAM simulations reduces the power spectrum of the MJO mode in wavenumber 1 but further extends it to wavenumber 1-5. CMT in MMF3DMF greatly reduces the power spectrum of easterly waves in Fig. 5f, which is also seen in Tulich (2015) that easterly wave signals are much weaker after incorporating the ESMT scheme in the SP-WRF simulations. Besides, the significant differences in the tropical wave spectrum between MMF2D and MMF3D in Fig. 5-6 could be associated with the structure of the background zonal flow. Tulich and Kiladis (2021) performed a series of aquaplanet simulations with axisymmetric structure of the background zonal winds through nudging, and concluded that nudging background zonal winds to match those over the Indo-Pacific or eastern Pacific sectors yields eastward-moving tropical waves (i.e., the moist Kelvin waves and the MJO) that are typically seen over those sectors.

By comparing with the CMT directly calculated from 3-D CRM flows in MMF3DMF, we verify the skill of the ESMT scheme in reproducing the spatial patterns and magnitude of CMT. Overall, the ESMT scheme readily captures the climatological mean horizontal and vertical profiles of both zonal and meridional components of CMT in Figs. 7-8 as well as its variability on high frequency, intraseasonal, and seasonal time scales in Fig. 9, but shows some differences in estimating their magnitudes. Such a difference is possibly related to the CRM orientation. Tulich (2015) found that the choice of CRM orientation

importantly affects the simulated time-mean climate due to changes in the explicit representation of wide-spread shallow convective regions. Cheng and Xu (2014) developed an explicit representation of CMT in MMF with the embedded 2-D CRM changing its orientation dynamically according to the vertical wind shear and thermal stratification, and obtained many improvements in mean climate and variability. The ESMT scheme captures the moderation effects of CMT by large-scale zonal winds and OLR in Fig. 10, although the modulation effects are less significant in comparison with MMF3DMF. It also captures the climatological mean vertical profile of CMT in Fig. 11 with positive momentum feedback in the lower/upper troposphereres and negative momentum feedback in the middle troposphere. Such a three-layer vertical structure of CMT was also found by Oh, Jiang, Waliser, Moncrieff, and Johnson (2015) based on the NOAA CFS reanalysis data. However, the ESMT scheme underestimates the variability of CMT in the middle troposphere.

Lastly, the MJO composite of zonal winds and CMT exhibits negative correlation in their horizontal profiles in Fig. 12 and vertical structure in Fig. 13 , decelerating zonal winds associated with the MJO and reflecting the cumulus friction effects of CMT. Similar deceleration effects were also found in the previous studies. Tung and Yanai (2002a) concluded that CMT on average is downgradient, reducing the large-scale vertical wind shear. That said, the signs of CMT near the surface is the same as the zonal winds in Fig. 13, accelerating the near-surface wind convergence and promoting convection. Similarly, Oh, Jiang, Waliser, Moncrieff, and Johnson (2015) concluded that the three-layer vertical structure of CMT damps the MJO circulation in the free troposphere, while enhancing MJO winds near the surface. Such a counter-gradient effect in accelerating near-surface westerly wind bursts was also emphasized in Moncrieff (2004). Yang, Majda, and Moncrieff (2019) proposed a basic parameterization for the counter-gradient effects of CMT from MCSs and improved the MJO simulations in an idealized GCM testbed. Kim and Zhang (2021) suggested that the strong Rayleigh damping in the MJO core dynamics could possibly be from CMT by moist convective processes.

The changes induced by implementing the ESMT scheme in E3SM-MMF highlights the important role of CMT in shaping large-scale circulation and convective organization. There are still several questions that are not addressed here but worth further investigation. For example, it should be interesting to study the skills of the CMT parameterization when the orientation of the CRMs are allowed to change with time and determined by environmental wind shear. It is also worth further investigating the relation between large-scale flows on

the GCM grids and small-scale flows in the CRM, illustrating the underlying mechanisms for the impact of CMT feedback. To exclude the effect of larger biases in MMF3D than those in MMF2D and demonstrate whether the ESMT scheme is indeed deficient in producing the CMT, a more straightforward way is to take a limited-area approach whereby the two embedded model types (i.e., 3-D CRM with explicit CMT versus 2-D CRM with ESMT) are subjected to the same large-scale forcing time series. This way, any differences in the predicted CMT effects can be attributed solely to differences in the model formulation. Alternatively, one could use E3SM-MMF with nudging of the large-scale circulation outside a region of interest, to avoid inherent issues due to imposed lateral boundary conditions in the limited area approach. Lastly, many insights from these MMF models should be also useful for improving CMT parameterizations in the non-MMF models. For example, the clear correlation between CMT and $U850$/FLNT in Fig. 10 reflects the crucial role of background lower-tropospheric winds and convective activities in modulating the magnitude and signs of CMT, indicating the essence of including these two controlling factors in the CMT parameterization. The countergradient effects of CMT on surface winds and the downgradient effects of CMT at higher levels in Fig. 13 highlight the essence of distinguishing different effects of CMT on vertical shear when developing CMT parameterizations.

7 Data Availability Statement

All code for E3SM may be accessed on the GitHub repository (https://github.com/E3SM-Project/E3SM). All code for E3SM-MMF may be accessed from a separate GitHub repository (https://github.com/E3SM-Project/ACME-ECP). The full code for the branch used in this study has been archive at W. Hannah (2022) (https://doi.org/10.5281/zenodo.6561445). The scripts and data for plotting all figures in this paper are available at Yang (2022) (`https://doi.org/10.5281/zenodo.6516010`). The ERA5 dataset for zonal winds can be downloaded from the Climate Data Store (CDS), including monthly averaged data (`https://cds.climate.copernicus.eu/cdsapp#!/dataset/reanalysis-era5-pressure-levels-monthly-means?tab=form`) and hourly data (`https://cds.climate.copernicus.eu/cdsapp#!/dataset/reanalysis-era5-pressure-levels?tab=form`). The IMERG dataset for precipitation can be downloaded from the NASA Goddard Earth Sciences (GES) Data and Information Services Center (DISC) website (`https://daac.gsfc.nasa.gov/datasets/GPM_3IMERGM_06/summary?keywords=IMERG`). The NOAA dataset for interpolated OLR

716 can be downloaded from the NOAA physical sciences laboratory (PSL) website (`https://`
717 `psl.noaa.gov/data/gridded/data.interp_OLR.html`).

718 **Acknowledgments**

719 This study was supported by the Exascale Computing Project (17-SC-20-SC), a collabo-
720 rative effort of the U.S. Department of Energy Office of Science and the National Nuclear
721 Security Administration. This research also used resources of the National Energy Research
722 Scientific Computing Center (NERSC), a U.S. Department of Energy Office of Science User
723 Facility operated under Contract DE-AC02-05CH11231. PNNL is operated for the Depart-
724 ment of Energy by Battelle Memorial Institute under contract DE-AC05-76RL01830. This
725 work was performed under the auspices of the U.S. Department of Energy by Lawrence
726 Livermore National Laboratory under Contract DE-AC52-07NA27344. This research used
727 resources of the Oak Ridge Leadership Computing Facility, which is a DOE Office of Science
728 User Facility supported under Contract DE-AC05-00OR22725.

729 ## References

730 Brenowitz, N., Majda, A., & Yang, Q. (2018). The multiscale impacts of organized convec-
731 tion in global 2-d cloud-resolving models. *JAMES*, *10*(8), 2009–2025.

732 Cheedela, S. K., & Mapes, B. E. (2019). Cumulus friction in the asian monsoon of a global
733 model with 7 km mesh. In *Current trends in the representation of physical processes*
734 *in weather and climate models* (pp. 197–205). Springer.

735 Cheng, A., & Xu, K.-M. (2014). An explicit representation of vertical momentum transport
736 in a multiscale modeling framework through its 2-d cloud-resolving model component.
737 *Journal of Geophysical Research: Atmospheres*, *119*(5), 2356–2374.

738 Dennis, J. M., Edwards, J., Evans, K. J., Guba, O., Lauritzen, P. H., Mirin, A. A., ...
739 Worley, P. H. (2012). Cam-se: A scalable spectral element dynamical core for the
740 community atmosphere model. *The International Journal of High Performance Com-*
741 *puting Applications*, *26*(1), 74–89.

742 Golaz, J.-C., Caldwell, P. M., Van Roekel, L. P., Petersen, M. R., Tang, Q., Wolfe, J. D.,
743 ... others (2019). The doe e3sm coupled model version 1: Overview and evaluation
744 at standard resolution. *JAMES*, *11*(7), 2089–2129.

745 Grabowski, W. W., & Moncrieff, M. W. (2001). Large-scale organization of tropical convec-
746 tion in two-dimensional explicit numerical simulations. *Quart. J. Roy. Meteor. Soc.*,

127(572), 445–468.

Gregory, D., Kershaw, R., & Inness, P. (1997). Parametrization of momentum transport by convection. ii: Tests in single-column and general circulation models. *Quart. J. Roy. Meteor. Soc.*, *123*(541), 1153–1183.

Hannah, W. (2022, May). *E3SMv2 branch used for Explicit Scalar Momentum Transport (ESMT) validation in E3SM-MMF.* Zenodo. Retrieved from `https://doi.org/10.5281/zenodo.6561445` doi: 10.5281/zenodo.6561445

Hannah, W., & Pressel, K. (2022). Transporting crm variance in a multiscale modelling framework. *EGUsphere*, *2022*, 1–25. Retrieved from `https://egusphere.copernicus.org/preprints/egusphere-2022-397/` doi: 10.5194/egusphere-2022-397

Hannah, W. M., Jones, C. R., Hillman, B. R., Norman, M. R., Bader, D. C., Taylor, M. A., ... others (2020). Initial results from the super-parameterized e3sm. *JAMES*, *12*(1).

Hannah, W. M., Pressel, K. G., Ovchinnikov, M., & Elsaesser, G. S. (2022). Checkerboard patterns in e3smv2 and e3sm-mmfv2. *Geoscientific Model Development Discussions*, *2022*, 1–24. Retrieved from `https://gmd.copernicus.org/preprints/gmd-2022-35/` doi: 10.5194/gmd-2022-35

Kershaw, R., & Gregory, D. (1997). Parametrization of momentum transport by convection. i: Theory and cloud modelling results. *Quart. J. Roy. Meteor. Soc.*, *123*(541), 1133–1151.

Khairoutdinov, M. F., & Randall, D. A. (2003). Cloud resolving modeling of the arm summer 1997 iop: Model formulation, results, uncertainties, and sensitivities. *J. Atmos. Sci.*, *60*(4), 607–625.

Kiladis, G. N., Wheeler, M. C., Haertel, P. T., Straub, K. H., & Roundy, P. E. (2009). Convectively coupled equatorial waves. *Rev. Geophys.*, *47*(2).

Kim, J.-E., & Zhang, C. (2021). Core dynamics of the mjo. *J. Atmos. Sci.*, *78*(1), 229–248.

Kuang, Z. (2008). A moisture-stratiform instability for convectively coupled waves. *JAS*, *65*(3), 834–854.

LeMone, M. A. (1983). Momentum transport by a line of cumulonimbus. *J. Atmos. Sci.*, *40*(7), 1815–1834.

LeMone, M. A., & Moncrieff, M. W. (1994). Momentum and mass transport by convective bands: Comparisons of highly idealized dynamical models to observations. *J. Atmos. Sci.*, *51*(2), 281–305.

Majda, A. J. (2007). New multiscale models and self-similarity in tropical convection. *J.*

Atmos. Sci., *64*(4), 1393–1404.

Majda, A. J., & Shefter, M. G. (2001). Models for stratiform instability and convectively coupled waves. *J. Atmos. Sci.*, *58*(12), 1567–1584.

Majda, A. J., & Stechmann, S. N. (2008). Stochastic models for convective momentum transport. *Proc. Natl. Acad. Sci. (USA)*, *105*(46), 17614–17619.

Majda, A. J., & Stechmann, S. N. (2009). A simple dynamical model with features of convective momentum transport. *J. Atmos. Sci.*, *66*(2), 373–392.

Mapes, B., Tulich, S., Lin, J., & Zuidema, P. (2006). The mesoscale convection life cycle: Building block or prototype for large-scale tropical waves? *Dyn. Atmos. Oceans*, *42*(1), 3–29.

Moncrieff, M. W. (1992). Organized convective systems: Archetypal dynamical models, mass and momentum flux theory, and parametrization. *Quart. J. Roy. Meteor. Soc.*, *118*(507), 819–850.

Moncrieff, M. W. (2004). Analytic representation of the large-scale organization of tropical convection. *J. Atmos. Sci.*, *61*(13), 1521–1538.

Moncrieff, M. W. (2019). Toward a dynamical foundation for organized convection parameterization in gcms. *Geophys. Res. Lett.*, *46*(23), 14103–14108.

Moncrieff, M. W., Liu, C., & Bogenschutz, P. (2017). Simulation, modeling, and dynamically based parameterization of organized tropical convection for global climate models. *J. Atmos. Sci.*, *74*(5), 1363–1380.

Oh, J.-H., Jiang, X., Waliser, D. E., Moncrieff, M. W., & Johnson, R. H. (2015). Convective momentum transport associated with the Madden–Julian oscillation based on a reanalysis dataset. *J. Climate*, *28*(14), 5763–5782.

Oh, J.-H., Jiang, X., Waliser, D. E., Moncrieff, M. W., Johnson, R. H., & Ciesielski, P. (2015). A momentum budget analysis of westerly wind events associated with the madden–julian oscillation during dynamo. *J. Atmos. Sci.*, *72*(10), 3780–3799.

Petersen, M. R., Asay-Davis, X. S., Berres, A. S., Chen, Q., Feige, N., Hoffman, M. J., ... others (2019). An evaluation of the ocean and sea ice climate of e3sm using mpas and interannual core-ii forcing. *JAMES*, *11*(5), 1438–1458.

Rappin, E. D., & Nolan, D. S. (2012). The effect of vertical shear orientation on tropical cyclogenesis. *Quart. J. Roy. Meteor. Soc.*, *138*(665), 1035–1054.

Richardson, Y. P., Droegemeier, K. K., & Davies-Jones, R. P. (2007). The influence of horizontal environmental variability on numerically simulated convective storms. part

i: Variations in vertical shear. *Mon. Wea. Rev.*, *135*(10), 3429–3455.

Richter, J. H., & Rasch, P. J. (2008). Effects of convective momentum transport on the atmospheric circulation in the community atmosphere model, version 3. *J. Climate*, *21*(7), 1487–1499.

Ringler, T., Petersen, M., Higdon, R. L., Jacobsen, D., Jones, P. W., & Maltrud, M. (2013). A multi-resolution approach to global ocean modeling. *Ocean Modelling*, *69*, 211–232.

Rotunno, R., Klemp, J. B., & Weisman, M. L. (1988). A theory for strong, long-lived squall lines. *J. Atmos. Sci.*, *45*(3), 463–485.

Schneider, E. K., & Lindzen, R. S. (1976). A discussion of the parameterization of momentum exchange by cumulus convection. *J. Geophys. Res.*, *81*(18), 3158–3160.

Taylor, K. E., Williamson, D., & Zwiers, F. (2000). *The sea surface temperature and sea-ice concentration boundary conditions for amip ii simulations*. Program for Climate Model Diagnosis and Intercomparison, Lawrence Livermore ....

Tulich, S. (2015). A strategy for representing the effects of convective momentum transport in multiscale models: Evaluation using a new superparameterized version of the weather research and forecast model (sp-wrf). *JAMES*, *7*(2), 938–962.

Tulich, S., & Kiladis, G. (2021). On the regionality of moist kelvin waves and the mjo: The critical role of the background zonal flow. *JAMES*, *13*(9), e2021MS002528.

Tung, W.-W., & Yanai, M. (2002a). Convective momentum transport observed during the TOGA COARE IOP. part I: General features. *J. Atmos. Sci.*, *59*(11), 1857–1871.

Tung, W.-W., & Yanai, M. (2002b). Convective momentum transport observed during the TOGA COARE IOP. part II: Case studies. *J. Atmos. Sci.*, *59*(17), 2535–2549.

Wheeler, M., & Kiladis, G. N. (1999). Convectively coupled equatorial waves: Analysis of clouds and temperature in the wavenumber–frequency domain. *J. Atmos. Sci.*, *56*(3), 374–399.

Woelfle, M., Yu, S., Bretherton, C., & Pritchard, M. (2018). Sensitivity of coupled tropical pacific model biases to convective parameterization in cesm1. *JAMES*, *10*(1), 126–144.

Wu, X., Liang, X.-Z., & Zhang, G. J. (2003). Seasonal migration of itcz precipitation across the equator: Why can't gcms simulate it? *Geophys. Res. Lett.*, *30*(15).

Wu, X., & Yanai, M. (1994). Effects of vertical wind shear on the cumulus transport of momentum: Observations and parameterization. *J. Atmos. Sci.*, *51*(12), 1640–1660.

Yang, Q. (2022, May). *Convective Momentum Transport and its Impact on the Madden-*

Julian Oscillation in E3SM-MMF. Zenodo. Retrieved from `https://doi.org/10.5281/zenodo.6516010` doi: 10.5281/zenodo.6516010

Yang, Q., & Majda, A. J. (2017). Upscale impact of mesoscale disturbances of tropical convection on synoptic-scale equatorial waves in two-dimensional flows. *J. Atmos. Sci.*, *74*(9), 3099–3120.

Yang, Q., & Majda, A. J. (2018). Upscale impact of mesoscale disturbances of tropical convection on convectively coupled kelvin waves. *J. Atmos. Sci.*, *75*(1), 85–111.

Yang, Q., & Majda, A. J. (2019). Upscale impact of mesoscale disturbances of tropical convection on 2-day waves. *J. Atmos. Sci.*, *76*(1), 171–194.

Yang, Q., Majda, A. J., & Brenowitz, N. D. (2019). Effects of rotation on the multiscale organization of convection in a global 2d cloud-resolving model. *J. Atmos. Sci.*, *76*(11), 3669–3696.

Yang, Q., Majda, A. J., & Moncrieff, M. W. (2019). Upscale impact of mesoscale convective systems and its parameterization in an idealized gcm for an MJO analog above the equator. *Journal of the Atmospheric Sciences*, *76*(3), 865–892.

Zhang, C., & Ling, J. (2017). Barrier effect of the indo-pacific maritime continent on the MJO: Perspectives from tracking mjo precipitation. *J. Climate*, *30*(9), 3439–3459.

Zhang, G. J., & Cho, H.-R. (1991a). Parameterization of the vertical transport of momentum by cumulus clouds. part ii: Application. *J. Atmos. Sci.*, *48*(22), 2448–2457.

Zhang, G. J., & Cho, H.-R. (1991b). Parameterization of the vertical transport of momentum by cumulus clouds. part i: Theory. *J. Atmos. Sci.*, *48*(12), 1483–1492.